DEUTSCHES ELEKTRONEN-SYNCHROTRON DESY

DESY 86-024
February 1986

PARTICLE TRACKING

by

H. Mais, G. Ripken and A. Wrulich
Deutsches Elektronen-Synchrotron DESY, Hamburg

F. Schmidt
II. Physikalisches Institut der Universität, Hamburg

ISSN 0418-9833

NOTKESTRASSE 85 · 2 HAMBURG 52

To be sure that your preprints are promptly included in the
HIGH ENERGY PHYSICS INDEX ,
send them to the following address (if possible by air mail) :

DESY
Bibliothek
Notkestrasse 85
2 Hamburg 52
Germany

DESY 86-024
February 1986

ISSN 0418-9833

PARTICLE TRACKING

H. Mais, G. Ripken and A. Wrulich*)
Deutsches Elektronen-Synchrotron DESY, Hamburg

F. Schmidt
II. Physikal. Inst. der Univ. Hamburg, D-2000 Hamburg

*) Present address: SSC, LBL, Univ. Res. Assoc., Univ. of California, Berkeley, USA

PARTICLE TRACKING

H. Mais, G. Ripken and A. Wrulich*)
DESY, Notkestraße 85, D-2000 Hamburg 52

F. Schmidt
II. Physikal. Inst. der Univ. Hamburg, D-2000 Hamburg

ABSTRACT

After a brief description of typical applications of particle tracking in storage rings and after a short discussion of some limitations and problems related with tracking we summarize some concepts and methods developed in the qualitative theory of dynamical systems. We show how these concepts can be applied to the proton ring HERA.

1. Introduction

The aim of the present talk is to discuss some applications and limitations of particle tracking in storage rings[1,2,3].

Although collective phenomena, as for example instabilities, are very important for accelerators we restrict ourselves to the single particle dynamics, i.e. we study the equations of motion of a single charged ultrarelativistic ($v \approx c$) particle under the influence of external electromagnetic fields. In general, these equations are nonlinear. The main nonlinearities are due to the beam-beam interaction, due to nonlinear cavity fields or due to transverse multipole fields. These multipole fields are either introduced artificially e.g. by sextupoles which compensate the natural chromaticity or they occur naturally as deviations from linear fields due to errors. Since the beam-beam interaction will be treated in extra seminars we shall not consider it here. We shall also not consider effects which are induced by radiation such as radiation damping and quantum excitations which are very important for light particles like electrons and positrons. In proton storage rings these effects can approximately be neglected. The radiation losses of a proton in HERA for example are a factor 10^{-7} less than the losses of the electron.

2. Hamiltonian description of the proton motion

Starting point for the proton dynamics is the following relativistic Lagrangian for a charged particle under the influence of an electromagnetic field described by a vector potential $\underline{A}(\underline{r}, t)$[4]

$$L = - m_0 c^2 \sqrt{1 - \dot{\underline{r}}^2/c^2} + \frac{e}{c} \dot{\underline{r}}\, \underline{A}(\underline{r}, t) \; . \qquad (1)$$

Usually, one changes to a Hamiltonian description of motion and one introduces the curvilinear coordinate system depicted in Fig. 1.

*) Present address: SSC, LBL, Univ. Res. Assoc., University of California, Berkeley, USA.

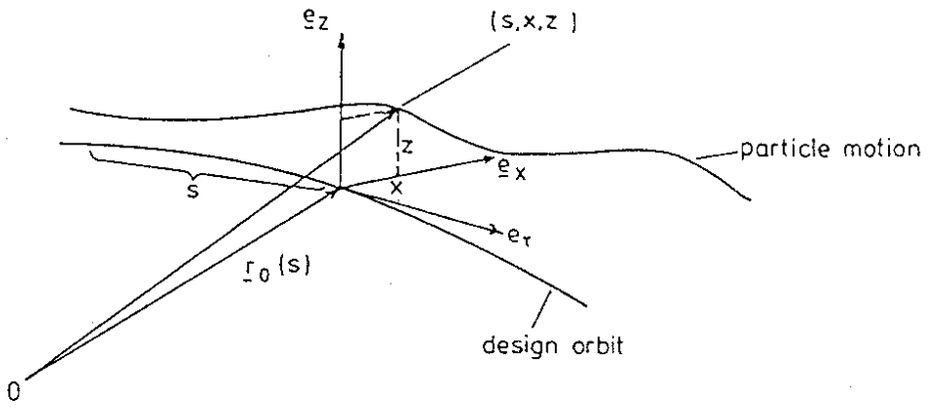

Fig. 1 Curvilinear coordinate system

It consists of three unit vectors $\underline{e}_\tau$, $\underline{e}_x$, $\underline{e}_z$ attached to the design orbit of the storage ring, s is the pathlength along this trajectory. For simplicity, we have assumed a plane reference orbit with horizontal curvature $\varkappa$ only. Using s as an independent variable and introducing difference variables with respect to an equilibrium particle on the design orbit one obtains ($v \approx c$, $\sigma = s - ct$, $p_\sigma = \frac{\Delta E}{E_0}$)

$$H = -(1+\varkappa x)\cdot\left\{(1+p_\sigma)^2 - (p_x - \frac{e}{E_0}A_x)^2 - (p_z - \frac{e}{E_0}A_z)^2\right\}^{1/2} - (1+\varkappa x)\frac{e}{E_0}A_\tau + (1+p_\sigma) \qquad (2)$$

with the corresponding equations of motion

$$\begin{cases} \frac{dx}{ds} = \frac{\partial H}{\partial p_x} \quad ; \quad \frac{dp_x}{ds} = -\frac{\partial H}{\partial x} \\ \frac{dz}{ds} = \frac{\partial H}{\partial p_z} \quad ; \quad \frac{dp_z}{ds} = -\frac{\partial H}{\partial z} \\ \frac{d\sigma}{ds} = \frac{\partial H}{\partial p_\sigma} \quad ; \quad \frac{dp_\sigma}{ds} = -\frac{\partial H}{\partial \sigma} \end{cases} \qquad (3)$$

and $\underline{A} = (A_\tau, A_x, A_z)$ satisfying Maxwell's equations.

By expanding the square root in equation (2) and the vector potential $\underline{A}$ into a Taylor series various examples for nonlinear motion can be investigated.

Example 1: Nonlinear cavity fields

$$H = \frac{1}{2} p_x^2 + \frac{1}{2} p_z^2 + \frac{g_0}{2} (x^2 - z^2) +$$

$$+ \frac{1}{2} \varkappa^2 x^2 - \varkappa x p_\sigma + V(s) \cos\sigma \qquad (4)$$

with $g_0 = \frac{e}{E_0} \left(\frac{\partial B_z}{\partial x}\right)_0$, $V(s) \equiv$ cavity voltage.

Introducing the dispersion function D defined by

$$D'' = - (\varkappa^2 + g_0) D + \varkappa \qquad (' \hat{=} \frac{d}{ds}) \qquad (5)$$

via the canonical transformation[5,6,7]

$$F_2 = \bar{p}_x (x - \bar{p}_\sigma D) + \bar{p}_\sigma D' x + \bar{p}_\sigma \sigma + \bar{p}_z z - \frac{1}{2} DD' \bar{p}_\sigma^2 \qquad (6)$$

one obtains

$$\bar{H} = \frac{1}{2} \bar{p}_x^2 + \frac{1}{2} (g_0 + \varkappa^2) \bar{x}^2 +$$

$$+ \frac{1}{2} \bar{p}_z^2 - \frac{1}{2} g_0 \bar{z}^2 -$$

$$- \frac{1}{2} \varkappa D \bar{p}_\sigma^2 + V(s) \cos(\bar{\sigma} + D\bar{p}_x - D'\bar{x}) \; . \qquad (7)$$

If there is no dispersion in the cavity region ($V(s)$ $D(s) \equiv 0$) the synchrotron motion (σ, p_σ) is completely decoupled from the betatron motion (x, P_x, z, p_z)[8]. In the case of a small dispersion one can write

$$\bar{H} \approx \frac{1}{2} \bar{p}_x^2 + \frac{1}{2} (g_0 + \varkappa^2) \bar{x}^2 +$$

$$+ \frac{1}{2} \bar{p}_z^2 - \frac{1}{2} g_0 \bar{z}^2 -$$

$$- \frac{1}{2} \varkappa D \bar{p}_\sigma^2 + V(s) \cos\bar{\sigma} -$$

$$- V(s) \cdot (D\bar{p}_x - D'\bar{x}) \sin\bar{\sigma} \; . \qquad (8)$$

Example 2: As a second example of nonlinear motion we consider the influence of transverse multipole fields with the following Hamiltonian:

$$H = \frac{1}{2} p_x^2 + \frac{1}{2} p_z^2 - \frac{e}{E_0} A_\tau(x, z) \; . \qquad (9)$$

The equations of motion are given by

$$x' = p_x$$

$$p_x' = \frac{e}{E_0}\frac{\partial A_\tau}{\partial x} = -\frac{e}{E_0} B_z(x, z)$$

$$z' = p_z$$

$$p_z' = \frac{e}{E_0}\frac{\partial A_\tau}{\partial z} = \frac{e}{E_0} B_x(x, z) \qquad (10)$$

with $$(B_z + iB_x) = B_0 \sum_{n=2}^{\infty} (b_n + ia_n)(x + iz)^{n-1} \quad .$$

The equations of motion in these two examples are highly nonlinear, and in general they cannot be solved analytically.

3. Dynamic aperture

One of the most important topics in accelerator physics one has to study is the dynamic aperture. This is an effective aperture of particle motion, beyond which the particle motion becomes unstable due to the nonlinear magnetic field. Figure 2 shows the ideal case where the dynamic aperture is almost the same as the physical aperture defined mainly by the size of the vacuum chamber.

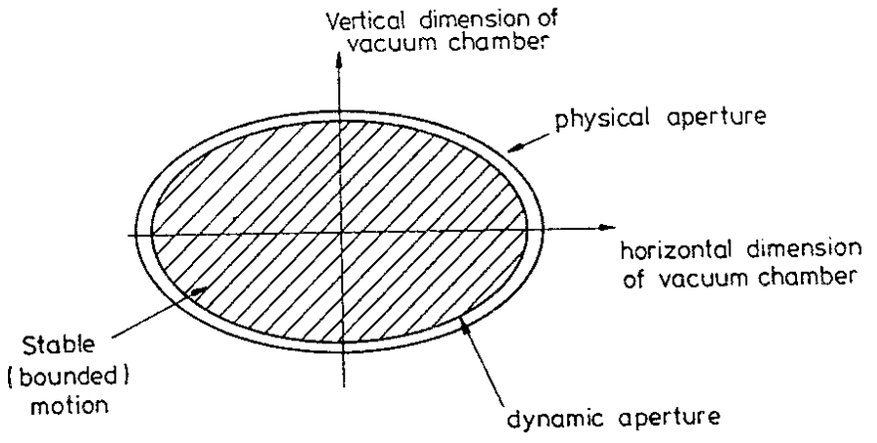

Fig. 2 Dynamic aperture, physical aperture

Among the questions for study are:

i) Is it possible to calculate and predict the dynamic aperture and how can this be done?

ii) How does it depend on the nonlinearities (multipole distribution, spatial distribution)?

iii) How does it depend on tunes? closed orbit distortions?

Tracking codes have been widely used to investigate these problems.

4. Particle tracking

The main idea of these codes is to track particles over many revolutions in a realistic model of the storage ring and to observe the amplitude of the particle at a special point s_0. Given the initial amplitude $\underline{y}(s_0) = (x(s_0), p_x(s_0), z(s_0), p_z(s_0), \sigma(s_0), p_\sigma(s_0))$ one needs to know $\underline{y}(s_0 + nL)$ (L = circumference of the accelerator) for n of the order of 10^9 (corresponding to a storage time of a particle of about 10 hours in HERA). Different methods and codes have been developed to evaluate $\underline{y}(s_0 + nL)$. Among others there are MARYLIE[9], TRANSPORT[10], RACETRACK[11] and PATRICIA[12]. The last two codes are kick codes where the nonlinear elements are replaced by δ-kicks according to:

$$a_{nm}(s)\, x^n z^m \longrightarrow \overline{a}_{nm}\, x^n z^m \cdot \delta(s - s_\nu) \quad . \tag{11}$$

In all cases mentioned the problem is reduced to the study of nonlinear symplectic mappings of the form:

$$\underline{y}(s_0 + nL) = \underline{T}(\underline{y}(s_0 + (n-1) \cdot L)) \tag{12}$$

or in shorthand notation

$$\underline{y}(n) = \underline{T}(\underline{y}(n-1)) \quad . \tag{12a}$$

The dimension of the mapping (dimension of $\underline{y}$) can vary from two to six according to the effects one has included (pure x- or z-motion, coupled betatron (x-z) motion, completely coupled synchro-betatron motion).

As an example for a kick code we briefly describe RACETRACK[11], which is a fast computer code to treat transverse magnetic multipole fields up to 20 poles. Several additional features, such as linear optics calculations, chromaticity adjustment, tune variation, orbit adjustment and inclusion of synchrotron oscillations are available. A schematic flow diagram is shown in Fig. 3.

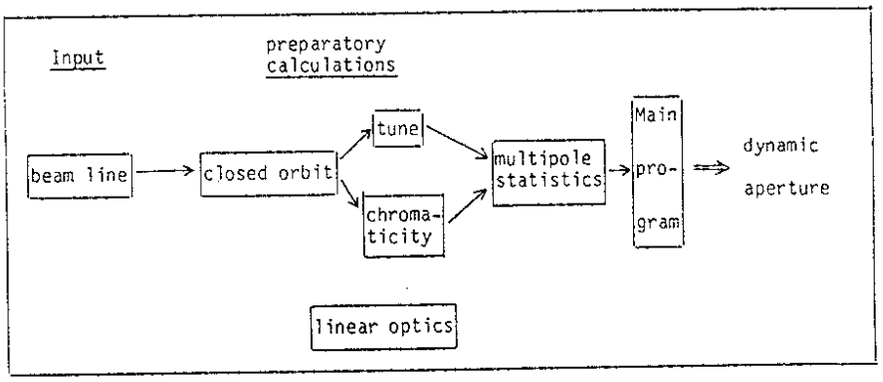

Fig. 3 Flow diagram of RACETRACK

Typical examples for the dynamic aperture of HERA obtained with RACETRACK are shown in Figs. 4 and 5[3] (four-dimensional coupled betatron case).

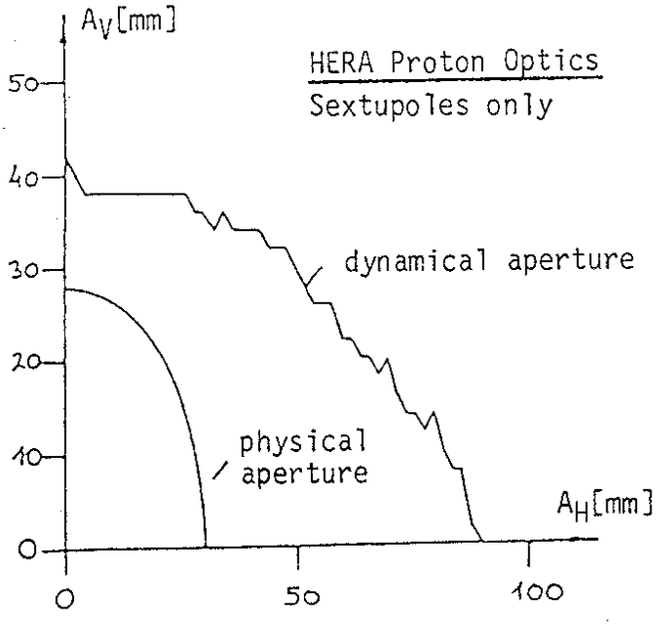

Fig. 4 Stable amplitude area

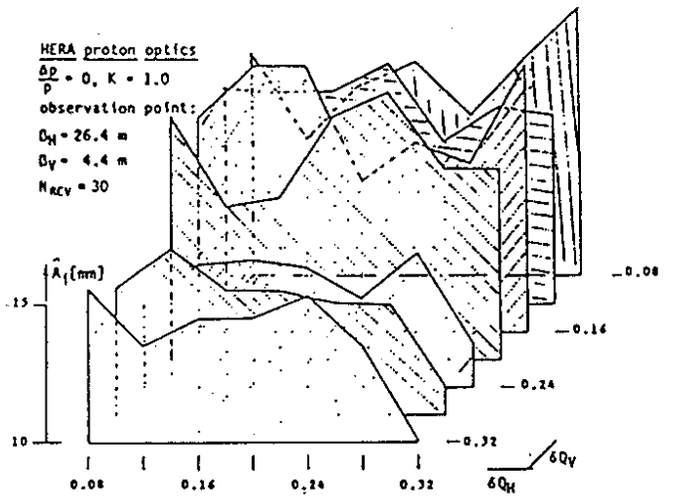

Fig. 5 Stable initial amplitude as a function of fractional tune

The main problems with tracking codes are the unavoidable rounding errors of the computers and the limited CPU-time. The rounding errors depend on the number system used by the compiler and they can destroy the symplectic structure of the nonlinear mappings. Thus, these rounding errors can simulate non-physical damping effects[1]. In order to estimate the order of magnitude of these effects one can switch to a higher precision structure in the computer hardware or software and observe the differences. Another way is to compare the differences between forward tracking of the particle and backward tracking[13]. The limited CPU-time restricts the number of revolutions one can track to about 10^6 (10^6 revolutions in HERA with multipole errors require a CPU-time in the order of days on an IBM 3081 K).

Besides these technical problems there are also some physical problems related with the evaluation and interpretation of the tracking data. For example, fast instabilities with an exponential increase of amplitudes beyond a certain boundary can easily be detected whereas slow, diffusion like processes which become dangerous only after 10^5 or 10^6 revolutions are much more difficult to detect.

Nevertheless tracking is the only way to obtain realistic estimates for the dynamic aperture up to 10^5 - 10^6 revolutions, but it is very difficult to extrapolate these data to longer times (10^9 revolutions and more).

In order to get maximum information out of these numerical simulations and for a better understanding of the underlying physics one should also apply analytical (perturbation) methods[14]. To understand how nonlinear systems might develop one should also know some of the results of the qualitative theory of dynamical systems.

5. Qualitative theory of dynamical systems

Although there are excellent review articles on this field[14,15,16,17,18] we summarize some important results in order to make this talk as selfcontained as possible.

The reduction of a Hamiltonian system to a nonlinear mapping as done by tracking codes has been a well-known procedure since Poincaré (1890). Consider for example a two-dimensional Hamiltonian system without explicit time (s-) dependence $H(q_1,q_2,p_1,p_2)$. The corresponding phase space is four-dimensional, and since H itself is a constant of the motion the physically accessible phase space is three-dimensional. Consider a surface Σ in this three-dimensional space as depicted for example in Fig. 6.

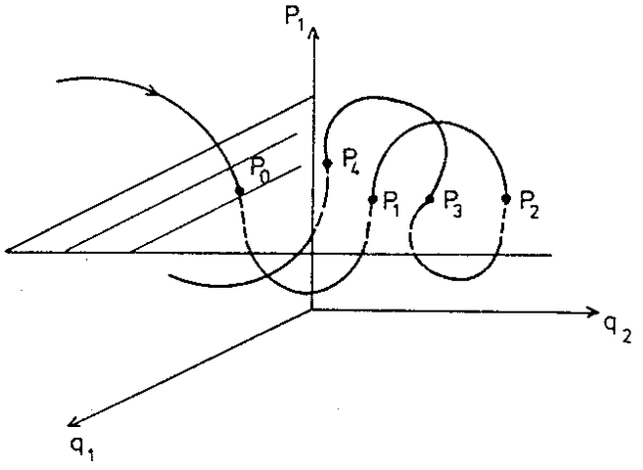

Fig. 6 Poincaré surface of section method

The bounded particle motion induced by the Hamiltonian H will generally intersect this surface in different points (P_0 ... P_3 ...). If one is not interested in the fine details of the orbit but only in the behaviour over longer time scales it is sufficient to consider the consecutive points $P_0 \longrightarrow P_1 \longrightarrow P_2 \longrightarrow \ldots$ of intersection. These contain complete information on the Hamiltonian system. In this sense one has reduced the Hamiltonian dynamics to a mapping of Σ to itself which is in general nonlinear (Poincaré surface of section technique). Similar mappings can also be derived for Hamiltonian systems with explicit periodic time-(s-)dependence (this is normally the case in storage rings).

Another important fact and, after the work of Chirikov[18], one of the few beacons among an otherwise still dense mist of diverse phenomena is the KAM-theorem (KOLMOGOROV, ARNOLD, MOSER; see for example Ref. 14). We will only illustrate this theorem in the two-dimensional case and instead of concentrating on mathematical rigour we will discuss its physical implications. Consider first the bounded motion of a two-dimensional autonomous (no explicit t- (s-) dependence) Hamiltonian System which is integrable. Roughly speaking, an n-dimensional system $H(q_1 \ldots q_n, p_1 \ldots p_n)$ is integrable if there exists a canonical transformation to action-angle variables $(I_1 \ldots I_n, \theta_1 \ldots \theta_n)$ such that the transformed Hamiltonian depends only on the n (constant) action variables $I_1 \ldots I_n$. For the considered two-dimensional case this implies that the motion is restricted to a two-torus parametrized by the two angle variables θ_1 and θ_2 as depicted in Fig. 7.

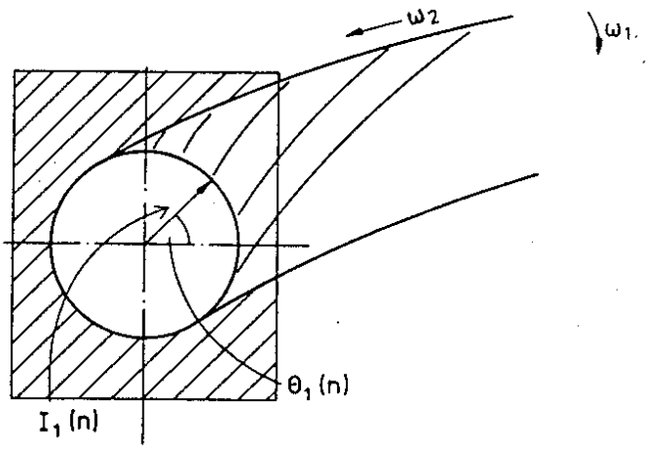

Fig. 7 Surface of section technique for an integrable system

As surface of section one can choose the $(I_1 - \theta_1)$-plane for θ_2 = const. In this surface of section which may be chosen to be just the plane of the page the motion of the integrable two-dimensional system looks very simple.

During the motion around the torus from one crossing of the plane to the next the radius of the torus (action variable) does not change,

$$I_1(n) = I_1(n-1) \ ,$$

and the angle θ_1 changes according to

$$\theta_1(n) = \theta_1(n-1) + \omega_1 \cdot T$$

where T is just the revolution time in θ_2-direction from one intersection of the plane to the next.

$$T = \frac{2\pi}{\omega_2} \quad .$$

Thus one obtains for an integrable system

$$I_1(n) = I_1(n-1)$$

$$\theta_1(n) = \theta_1(n-1) + 2\pi\alpha(I_1(n)) \quad . \tag{13}$$

The term α is the so-called winding number. It is the ratio of the two frequencies of the system and it generally depends on I_1. If α is irrational the $\theta_1(n)$ form a dense circle while if α is rational the $\theta_1(n)$ close after a finite sequence of revolutions (periodic orbit). Thus, there are invariant curves (circles) under the mapping which belong to rational and irrational winding numbers. What happens now if a perturbation is switched on, i.e. if

$$I_1(n) = I_1(n-1) + \epsilon f(I_1(n), \theta_1(n-1))$$

$$\theta_1(n) = \theta_1(n-1) + 2\pi\alpha(I_1(n)) + \epsilon g(I_1(n), \theta_1(n-1))\,? \tag{14}$$

In particular, can one still find invariant curves? The KAM-theorem says that this is indeed the case if the following conditions are fulfilled (together with some requirements of differentiability and periodicity for f and g; for more details see for example Ref. 14):

i) The perturbation must be weak

ii) $\alpha = \frac{\omega_1}{\omega_2}$ must be sufficiently irrational, i.e. $\left|\alpha - \frac{p}{q}\right| > \frac{K(\epsilon)}{q^{2+\delta}}$.

Under these assumptions most of the unperturbed tori survive the perturbation although in distorted form.

The rational and some nearby tori however are destroyed, only a finite number of fixed points of the rational tori survive - half of them are stable (elliptic orbits around this fixed point), half of them are unstable (hyperbolic orbits). The hyperbolic fixed points are the source of chaotic motion in phase space, i.e. motion which is extremely sensitive to the variation of initial conditions. The motion around the elliptic fixed points can be considered as motion around a torus with smaller radius and the arguments used till now can be repeated on this smaller scale giving rise to the schematic picture shown below.

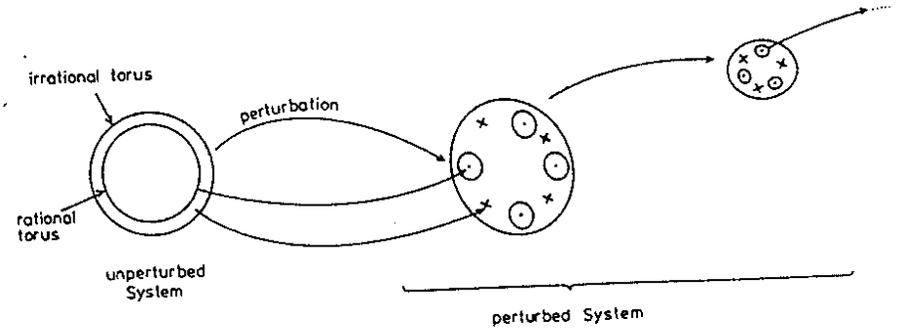

Fig. 8 Perturbation of an integrable system

Thus, the phase space pattern of a weakly perturbed integrable two-dimensional system looks extremely complicated. There are regular orbits confined to tori and among them are distributed chaotic trajectories in a delicate manner. One should point out at this stage that there are no analytical methods for calculating these chaotic orbits - perturbation theories diverge.

6. Studies of chaotic behaviour in HERA caused by transverse magnetic multipole fields

Now we would like to present numerical results using RACETRACK with special emphasis on finding and investigating chaotic trajectories in phase space[19,20]. The calculations have been performed on a 370 E Emulator and the IBM 3081 K. The number of revolutions was varied between 30000 and 300000 using a HERA proton optics with a fixed realistic multipole distribution of the kind resulting from nonlinear field errors in the superconducting magnets.

At first, we have studied purely horizontal motion (i.e. without coupling to the vertical betatron motion) which of course leads to a two-dimensional nonlinear mapping. Fig. 9 shows a $p_x - x$ plot of a particle trajectory near the dynamic aperture.

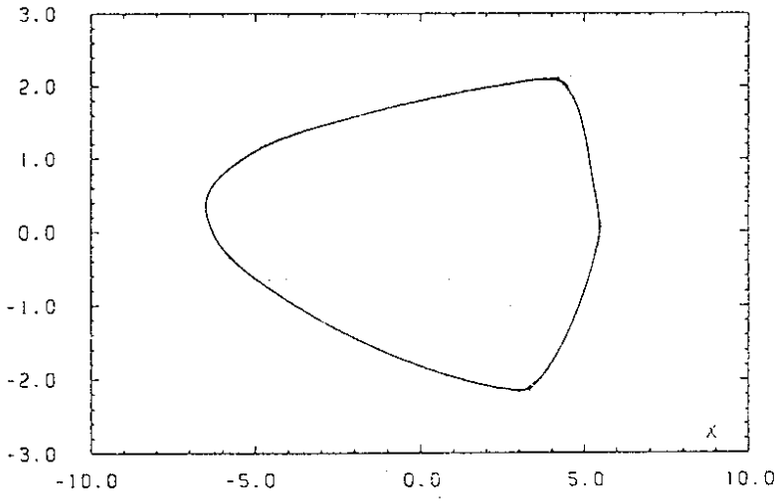

Fig. 9

In an enlarged scale one clearly sees the island structure around elliptic fixed points and the chaotic (area filling) behaviour near the hyperbolic fixed points (see Fig. 10).

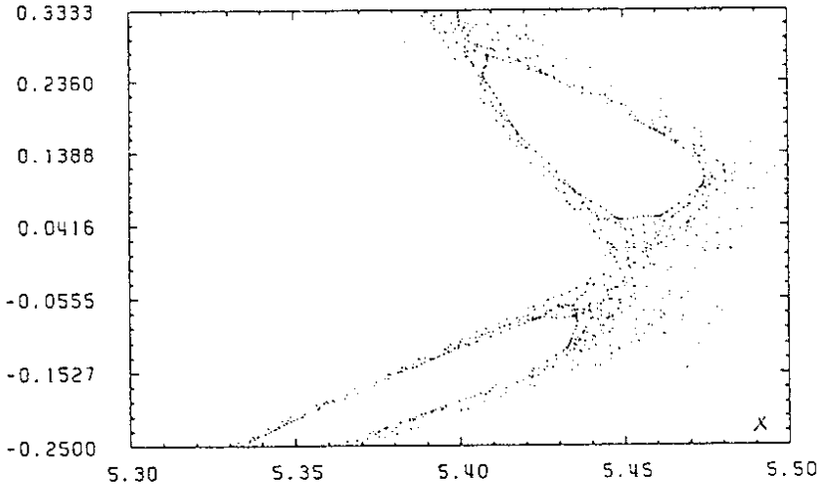

Fig. 10

In this two-dimensional case the dynamic aperture could be identified with the largest existing KAM-circle. There exist well-known methods for investigating the break-up of these border lines[21,22] whose disappearance with increasing perturbation would lead to a kind of global chaos, a situation one naturally wants to avoid in storage ring physics. In addition, two-dimensional systems are special in that the existence of KAM-circles implies exact stability. Since chaotic trajectories cannot escape without intersecting these invariant surfaces, they are forever trapped between these tori if they indeed exist.

This is not true for higher dimensional systems where the KAM-theorem predicts three-tori ($S_1 \times S_1 \times S_1$) in six-dimensional phase space, four-tori in eight dimensional phase space etc.

Here chaotic trajectories can in principle always escape although their motion can be obstructed strongly by these tori. Chaotic regions can even form a connected web along which the particle can diffuse as has been demonstrated by Arnold for a special example (Arnold diffusion, see for example[14]).

As a next step we consider the fully coupled x - z motion in HERA under the influence of the nonlinear multipole fields. There are several possibilities for displaying four-dimensional phase space trajectories. The simplest way is to draw projections onto the different planes (x,p_x), (z,p_z), (x,z), (p_x,p_z), (x,p_z) and (z,p_x) but one can also use three-dimensional projections and colour to represent the fourth variable[20].

In this higher dimensional case one cannot simply use the area filling property for distinguishing chaotic trajectories from regular ones, one needs some other characteristic features. One property of chaotic motion is the exponential separation of two phase space points which initially have been close together. Formally this can be described by the characteristic Lyapunov exponent[14]

$$\lambda = \lim_{\substack{d(o)\longrightarrow o \\ t\longrightarrow\infty}} \frac{1}{t} \ln \frac{|d(t)|}{|d(o)|} \qquad (15)$$

where d(t) describes how the (Euclidean) distance between two adjacent phase space points evolves with time and d(o) is the initial distance. Nonzero Lyapunov exponents are a quantitative measure for stochasticity of the considered trajectories.

Typical examples for regular and chaotic trajectories for HERA are shown in Figs. 11 to 22. We show the projections of these orbits onto the different planes.

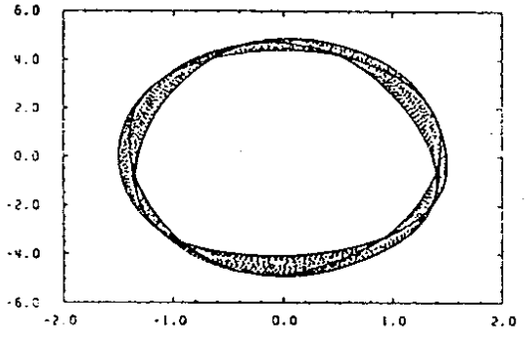

Fig. 11 P_z versus z (regular trajectory)

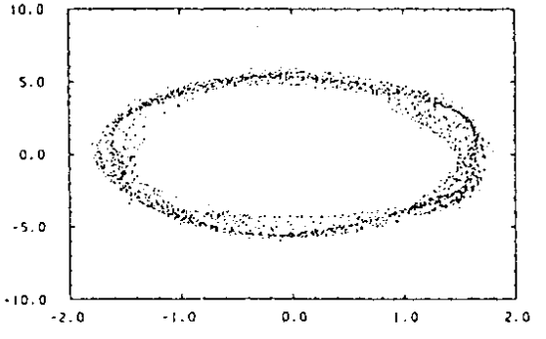

Fig. 12 P_z versus z (chaotic trajectory)

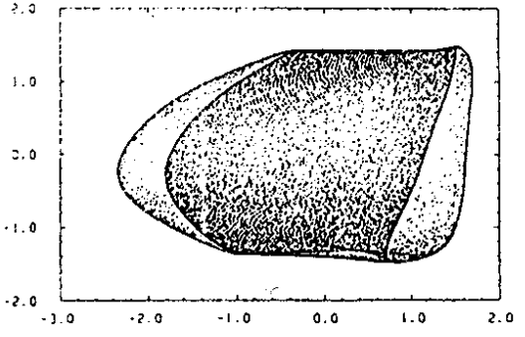

Fig. 13 x versus z (regular trajectory)

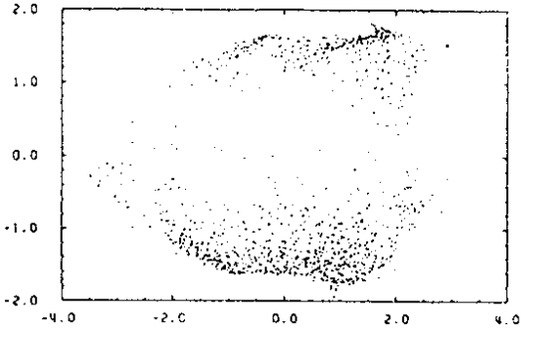

Fig. 14 x versus z (chaotic trajectory)

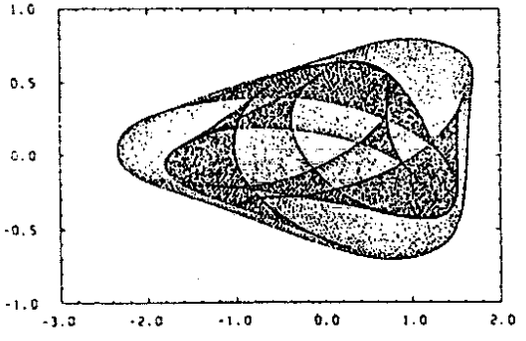

Fig. 15 P_x versus x (regular trajectory)

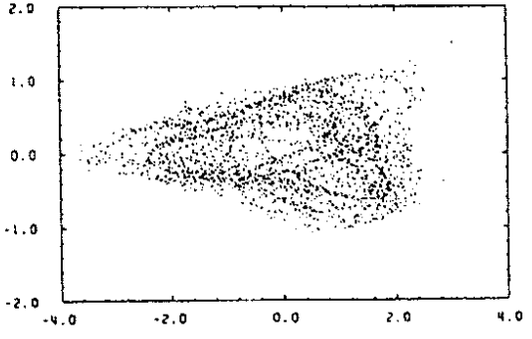

Fig. 16 P_x versus x (chaotic trajectory)

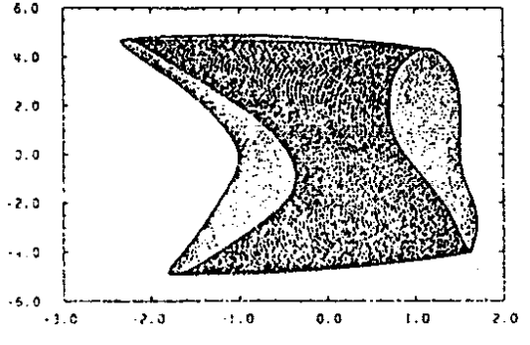

Fig. 17 x versus P_z (regular trajectory)

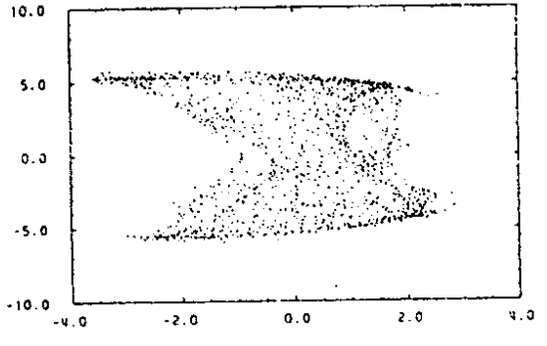

Fig. 18 x versus P_z (chaotic trajectory)

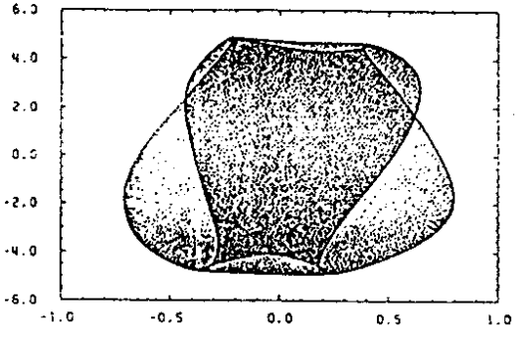

Fig. 19 P_x versus P_z (regular trajectory)

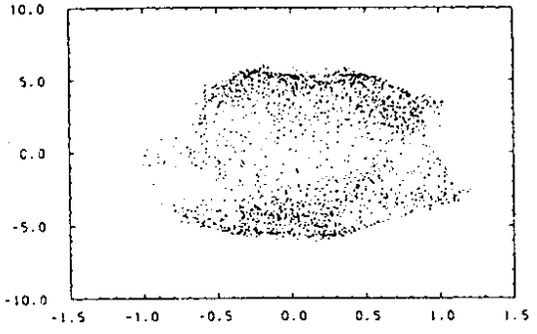

Fig. 20 P_x versus P_z (chaotic trajectory)

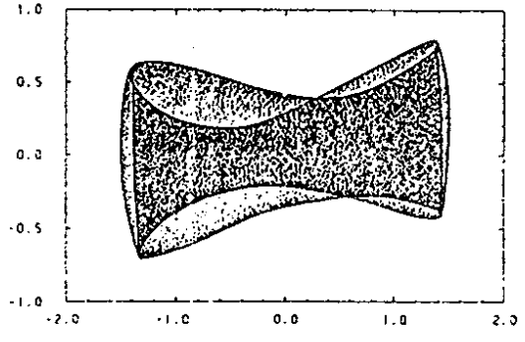

Fig. 21 z versus P_x (regular trajectory)

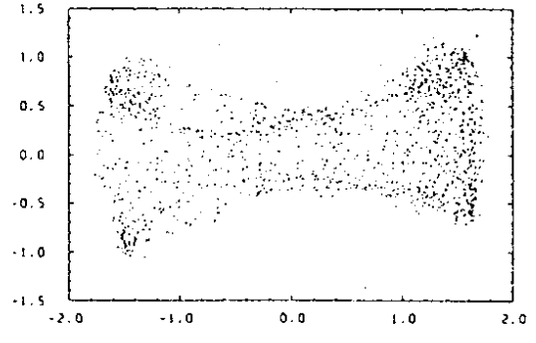

Fig. 22 z versus P_x (chaotic trajectory)

Figures 23 and 24 show how the distance between two adjacent phase space points evolves with time, first for a regular trajectory (linear increase) and second for a chaotic orbit (exponential increase).

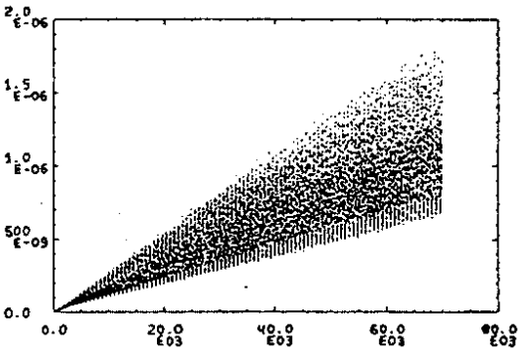

Fig. 23

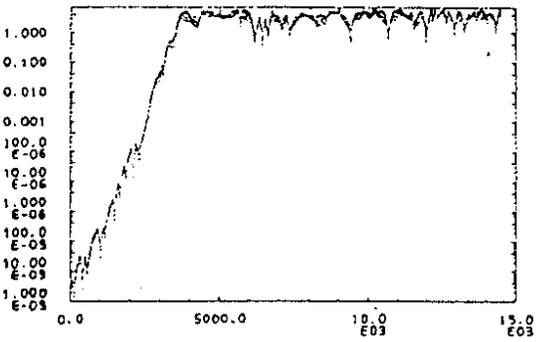

Fig. 24

7. Summary

Thus, HERA shows all the features which are characteristic for nonintegrable Hamiltonian systems. However, because of the possibility of Arnold diffusion the existence of tori does not imply global stability in the four-dimensional case (coupled betatron motion) contrary to the uncoupled case. Until now, these chaotic trajectories have been observed only near the dynamic aperture. However, it is not clear whether this is also true for the case of coupled synchro-betatron motion (six-dimensional mappings) and how relevant these chaotic regions are in practice. Further investigations in this direction and more computer experiments are certainly needed for a better understanding. In addition, the application of perturbation methods might be helpful in suggesting directions for further investigations and how to design these numerical experiments[23].

Recently interesting attemps have also been made to compare the theoretical and tracking predictions with machine experiments[24,25].

For future work it is also desirable to extend these investigations to include collective effects and spin effects. Promising attemps have been made already[26,27,28] but many questions are still open.

Acknowledgements

It is a pleasure to thank our colleagues at DESY Dr. D.P. Barber, Dr. R. Brinkmann and Dr. F. Willeke for many helpful discussions.

References

1) R.V. Servranckx, Proc. Part. Accel. Conf., Vancouver 1985, IEEE Trans. Nucl. Sci. NS-32, 2186 (1985).

2) E. Keil, CERN 84-01, 1984.

3) A. Wrulich, DESY HERA 84-07, 1984.

4) G. Ripken, DESY 85-084, 1985.

5) H. Mais, G. Ripken, DESY Report to be published.

6) C.J.A. Corsten, H.L. Hagedoorn, Nucl. Instr. Meth. 212, 37 (1983).

7) T. Suzuki, Part. Accel. 12, 237 (1982).

8) A. Piwinski, these proceedings.

9) A.J. Dragt, D.R. Douglas, E. Forest, L.M. Healy, F. Neri, R.D. Ryne, Proc. Part. Accel. Conf, Vancouver 1985, IEEE Trans. Nucl. Sci. NS-32, 2311 (1985).

10) K.L. Brown, D.C. Carey, C. Iselin, F. Rothacker, CERN 80-04, 1980.

11) A. Wrulich, DESY 84-026, 1984.

12) H. Wiedemann, PEP Note 220, SLAC, 1976.

13) P. Wilhelm, Diploma Thesis Univ. of Hamburg, 1985.

14) A.J. Lichtenberg, M.A. Lieberman, Regular and stochastic motion, Springer, New York, Berlin 1983.

15) M.V. Berry, American Institute of Physics, Conf. Proc. No. 46, 1978.

16) R.H.G. Helleman, Fundamental problems in statistical mechanics V, North Holland Publ. Co. 1980.

17) M. Hénon, Chaotic behaviour of deterministic systems, North Holland Publ. Co. 1983.

18) B.V. Chirikov, Physics Reports 52, 263 (1979).

19) H. Mais, F. Schmidt, A. Wrulich, Proc. Part. Accel. Conf. Vancouver 1985, IEEE Trans. Nucl. Sci. NS-32, 2252 (1985).

20) F. Schmidt, private communication and PhD-thesis Univ. of Hamburg, to be published.

21) J.M. Greene, J. Math. Phys. 20, 1183 (1979).

22) R.S. MacKay, Renormalisation in area preserving maps, Dissertation, Princeton University, 1982.

23) F. Willeke, FERMILAB FN-422, 1985.

24) D.A. Edwards, R.P. Johnson, F. Willeke, FERMILAB-Pub-85/59, 1985.

25) P.L. Morton, J.H. Pellegrin, T. Raubenheimer, L. Rivkin, M. Ross, R.D. Ruth, W.L. Spence, Proc. Part. Accel. Conf., Vancouver 1985, IEEE Trans. Nucl. Sci. NS-32, 2291 (1985).

26) R.H. Siemann, American Institute of Physics, Conf. Proc. No. 127, 1985.

27) J. Kewisch, DESY 85-109, 1985.

where $(\bar{q}_f(x))q_f(x)$ is the (anti)-quark density for a given flavor f inside the proton and $A_f^{(2,3)}$ are coefficients which depend on the e.w. charges and the W,Z propagators. It is summed over all active flavors. To be more specific, in the CC case one simply has

$$A_f^{(2)} = A_f^{(3)} = \left[4 \sin^2\theta_w \left(1 + m_w^2/Q^2\right)\right]^{-2}, \qquad (19)$$

while f runs over all positively ($e^- p \to \nu_e X$) or negatively ($e^+ p \to \bar{\nu}_e X$) charged quarks and antiquarks. Apart from the trivial Q^2-dependence due to the weak boson propagators, the structure functions eq. (18) depend only on the parton momentum fractions x. This is the scaling limit [38]. As everybody knows, the color interactions of quarks and gluons induce logarithmic violations of scaling. A particularly transparent representation of this fact is provided by the Altarelli-Parisi equations [40] for the quark and gluon densities. Schematically,

$$\frac{\partial q(x,Q^2)}{\partial \ln Q^2} = \frac{\alpha_s(Q^2)}{2\pi} \int_x^1 \frac{dz}{z} \left[q(z,Q^2) P_{qq}\left(\frac{x}{z}\right) + G(z,Q^2) P_{qg}\left(\frac{x}{z}\right)\right]$$

$$\frac{\partial G(x,Q^2)}{\partial \ln Q^2} = \frac{\alpha_s(Q^2)}{2\pi} \int_x^1 \frac{dz}{z} \left[\sum_q q(z,Q^2) P_{gq}\left(\frac{x}{z}\right) + G(z,Q^2) P_{gg}\left(\frac{x}{z}\right)\right] \qquad (20)$$

where $\alpha_s(Q^2)$ is the effective coupling constant of QCD. The socalled splitting functions $P_{ab}(z)$ describe the momentum distribution of a "parton b inside a parton a" and can be derived from the fundamental vertices of QCD. In short, the scaling violations are determined by

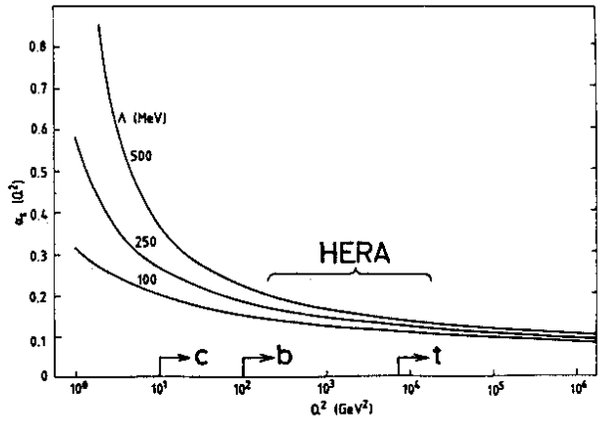

Fig. 12. The running coupling constant of QCD in two-loop approximation for various values of the QCD scale Λ including heavy quark thresholds (from ref. 3)

the running of α_s with Q^2 and by anomalous dimensions related to moments of the splitting functions. The running of $\alpha_s(Q^2)$ is demonstrated in Fig. 12. One observes that, irrespectively of uncertainties in Λ which at present scales are due to non-perturbative effects [41], $\alpha_s(Q^2)$ is predicted rather precisely in the Q^2 range of HERA. Consequently, it will not be possible at HERA to fix Λ accurately, however, one can undoubtedly check the correct running of $\alpha_s(Q^2)$ starting from the values measured at low scales.

Similarly, quantitative tests of the QCD scaling violations at present energies [41] are affected by uncertainties concerning higher twist operators, target mass and charm threshold effects, and other non-perturbative contributions. This background is expected to fall off like a power in Q^2 and, hence, should disappear much faster than the genuine QCD signal as Q^2 increases. Therefore, by establishing contact with the structure functions measured at present energies and following their evolution up to the highest possible values of Q^2 at HERA, one can be confident to provide one of the most relevant QCD tests. This assertion assumes that electroweak effects (charges, propagators, radiation) as well as heavy flavor thresholds (b-quark) are carefully taken into account. Some manipulations [35,42] are required in order to bridge the formal differences of today's (isoscalar target) and HERA's (proton target) structure functions. The statistics itself is not a problem as illustrated in Fig. 13. Finally, although the usable low Q^2 range at HERA is limited by large errors in x and Q^2 measurements in this region of phase space (Fig. 10), overlap in Q^2 with existing data can be accomplished by running at lower c.m. energies.

Another obvious task at HERA is the determination of quark and gluon densities, in particular, at large Q^2. This not only provides information on the structure of matter at 10^{-16} cm, but also solidifies the basis for analyses and predictions of physics at present and future hadron colliders. Whereas quark densities can be extracted from NC & CC structure functions [42], preferably measured at various c.m.

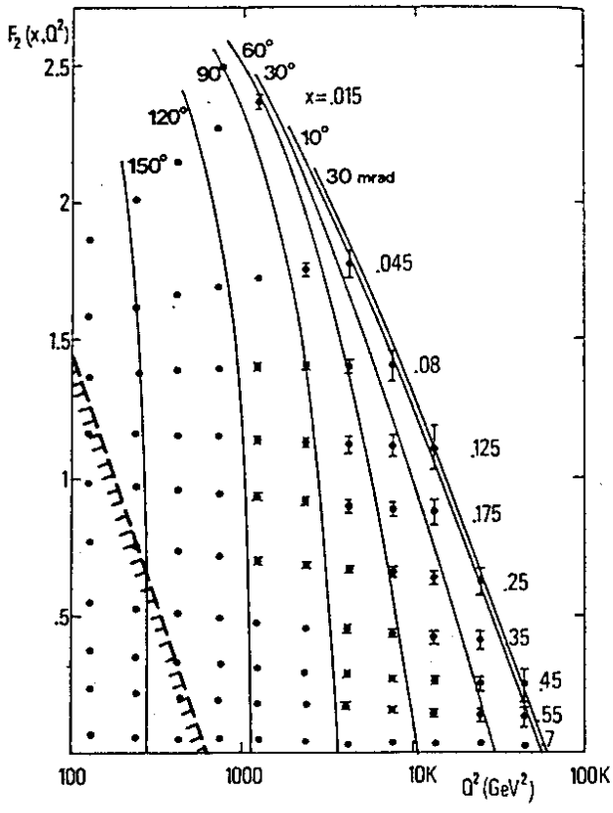

energies, the gluon density must be determined indirectly from the observed pattern of scaling violations. How successful one is in this respect at present energies, is nicely described in another talk [41] at this Conference. Just to indicate what one can optimistically expect from HERA, the quality of the constraints on $F_2 \sim x(q+\bar{q})$ and gluon density G at fixed Q^2 (resulting from QCD fits to NC-structure functions) is depicted in Fig. 14.

Fig. 13. QCD evolution exemplified by the structure function $F_2(x, Q^2 = 3\ GeV^2) \sim x(1-x)^3$. Also shown are statistical errors for a NC-run of 250 pb^{-1} at HERA. Continuous lines represent fixed final e angle. The low Q^2 region not accessible at the maximum HERA energy is indicated (from ref. 35).

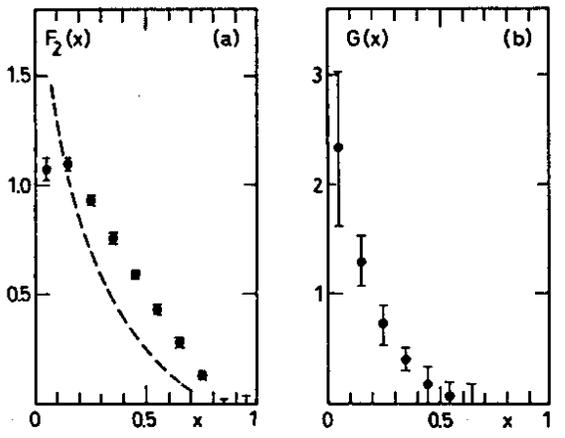

Fig. 14. Constraints on input x-distributions at $Q^2 = 3\ GeV^2$ from QCD fits to scaling violations for a very good detector. F_2 is as in previous figure and $G \sim (1-x)^5$. The dashed curve indicates F_2 evolved to $Q^2 \simeq 10^3\ GeV^2$ (from ref. 35).

Unfortunately, I have no time to discuss other topics of conventional physics [2,5] at HERA. It is however clear that systematic QCD studies must and will also include longitudinal structure func-

tions [35,41] ($F_L = F_2 - 2xF_1$), jets, [35,43] energy flow, [2,44], and last but certainly not least (gluon distribution!) photoproduction [32,36]. Needless to say, thorough consideration ought to be given to e.w. physics both as a "background" in QCD tests and as an own subject of great theoretical interest.

5.2 Quark Form Factors and New Interactions

Of course, experimentation at HERA would be even more exciting, if some effect signaling new physics were discovered. Suppose quarks are composite with a typical radius $r \sim 1/\Lambda$ while leptons are considerably more pointlike. In this case, [3] photons with $Q^2 < \Lambda^2$ would see quarks, i.e. $F_2 \sim \langle Q_q^2 \rangle \times Q(x)$, whereas photons with $Q^2 > \Lambda^2$ would resolve the preon substructure, i.e. $F_2 \sim \langle Q_p^2 \rangle \times P(x)$. Making, furthermore, the rather conservative assumptions that the preon structure of quarks is very similar to the quark structure of nucleons, $xQ \simeq 2(1-x)^3$, and that the quark-preon transition is described by a dipol form factor, $f(Q^2/\Lambda^2) = (1+Q^2/\Lambda^2)^{-2}$, one has the situation illustrated in Figs. 15 and 16. Considering the dramatic collapse of the parton densities towards small x (Fig. 15), it is at first sight a little surprising that there would be almost no effect in the structure functions at HERA (Fig. 16). The last statement can be turned into a maximum observable form factor scale, to wit $\Lambda \sim \sqrt{s} \sim 300$ GeV.

However, the situation can be quite different if quarks and leptons are composite at approximately the same scale Λ_H. In this case, one expects [45] residual 4-fermion interactions (Fig. 2) arising, for example, from the interchange of preons. The corresponding operators in $\mathcal{L}_{eff}$ have dimension 6 and, consequently, dimensionful effective couplings $\sim g^2/\Lambda_H^2$. Since the preon binding force is most likely strong, one may plausibly assume $g^2/4\pi = O(1)$. This then implies large signals in NC and CC cross sections and asymmetries [46] already at $Q^2 \ll \Lambda_H^2$ as exemplified by Figs. 17 and 18 for contact interactions of the form $\frac{g^2}{\Lambda_H^2} (\bar{e}e)_{LorR}(\bar{q}q)_{LorR}$. Here, $(\bar{\Psi}\Psi)_{L,R}$ denote usual left(right)-handed

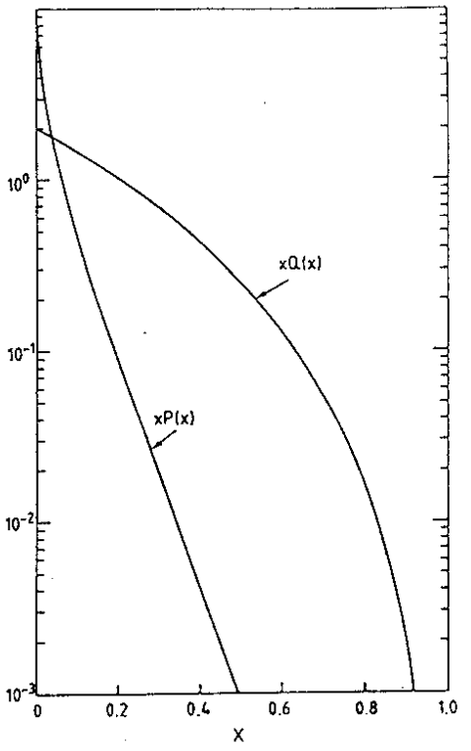

Fig. 15. Momentum distributions of quarks (xQ) and preons (xP) inside nucleons under the assumptions described in the text (from ref. 3)

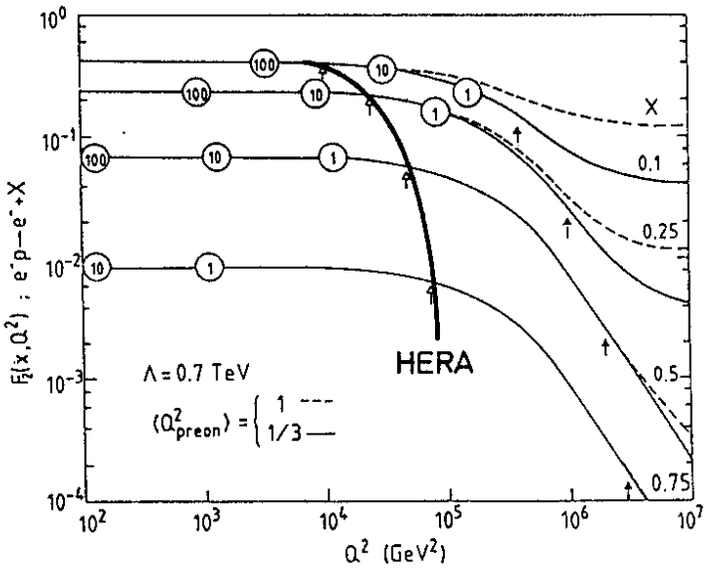

Fig. 16. Transition of the proton structure function F_2 from the quark to the preon scaling region for a compositeness scale $\Lambda = 0.7$TeV and a dipol form factor. The numbers in the circles are events per day assuming scaling, $\sqrt{s} = \infty$ and $\mathcal{L} = 10^{32}$ cm^{-2}s^{-1}. The actual phase space boundary of HERA is indicated (from ref. 3).

currents. One can see that HERA will probe compositeness of electrons and light quarks up to scales $\Lambda_H \sim$ (3-5) TeV. Remarkable [46] is also the sensitivity of asymmetries to the detailed Lorentz structure of contact interactions.

5.3 New Weak Currents and Bosons

Effective contact interactions may also arise from the exchange of new very heavy bosons. In particular, models for composite W and Z predict a whole spectrum of excited states with masses $M \sim O(\Lambda_H)$. However, these states are expected [31] to couple weakly, i.e. $g^2/4\pi \sim O(g_w^2/4\pi \simeq 10^{-2})$, in contrast to what was assumed in 5.2. Correspondingly, the above limit $\Lambda_H \lesssim$ (3-5) TeV has to be rescaled to $M \lesssim$ (300-500) GeV. This rough estimate is confirmed by more detailled

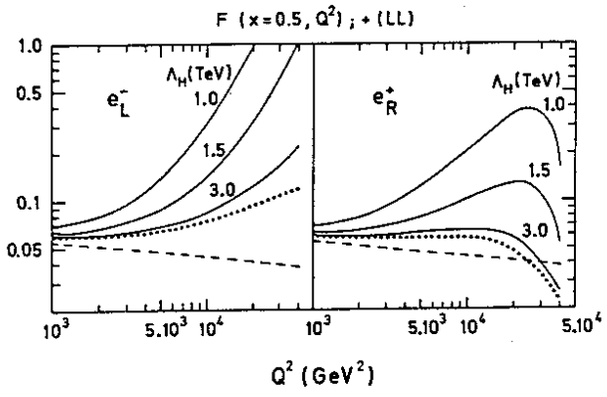

Fig. 17. The reduced cross section $F = \frac{d\sigma}{dxdy} \Big/ \frac{2\pi\alpha^2 s}{Q^4}\left(1+(1-y)^2\right)$ for polarized NC processes at HERA. The dashed curves expose the contributions from γ-exchange; the dotted curves display the full standard model predictions; the full curves include L•L contact terms for various values of Λ_H (from ref. 46).

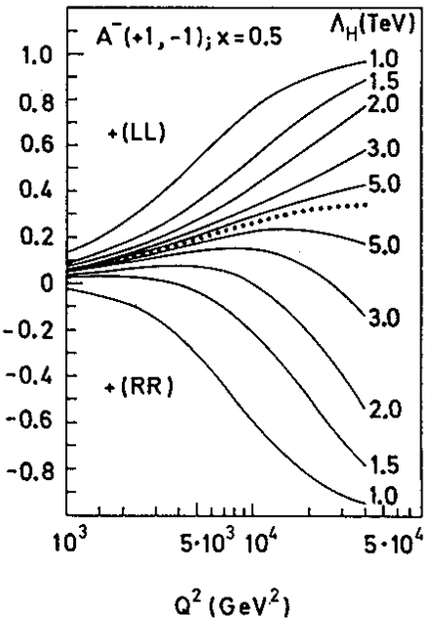

Fig. 18. Polarization asymmetry $A^-(+1,-1) = \frac{d\sigma_L - d\sigma_R}{d\sigma_L + d\sigma_R}$ for $e^-_{L,R}$ NC-scattering at HERA. The dotted curve is the standard model prediction, the full curves include L•L and R•R contact terms, respectively (from ref. 46).

model studies [3,4].

As a rather simple example, one can study new weak bosons W' and Z' which couple to ordinary leptons and quarks similarly as the known intermediate vector bosons do. If one requires a minimum effect of (20-30) % on cross sections or asymmetries at $Q^2 \gtrsim 10^4$ GeV in order to detect the signal, one can generally reach $M_{W',Z'} \sim 400$ GeV. It is also conceivable that the new bosons connect old (light) and new (heavy) fermions as indicated in Fig. 3a. Assuming the existence of heavy partners with degenerate masses for all flavors, one estimates a cross section [3] $\sigma(ep \to L^0QX) \simeq 0.1$ pb for $M_{W'} \simeq 400$ (200) GeV and $m_{L^0} \simeq m_Q \simeq 50(100)$ GeV. The decays of the heavy fermions produce multi-lepton/jet final states which constitute a good signature [4].

Perhaps more interesting is the conjecture [7] of the existence of new gauge bosons associated with a $SU(2)_R$ symmetry. Replacing the standard e.w. gauge group $SU(2)_L \times U(1)$ by $SU(2)_L \times SU(2)_R \times U(1)$ one can attempt to generate the observed P and C violations in weak interactions by spontaneous symmetry breaking. The usual $SU(2)_L$ fermion doublets become singlets under $SU(2)_R$, while the right-handed fermion components which are singlets under $SU(2)_L$ now become doublets under $SU(2)_R$. In particular, right-handed neutrinos ν_R appear as partners of the right-handed charged leptons. A discrete L-R symmetry enforces $g_L = g_R$ upon the $SU(2)_{L,R}$ couplings. After symmetry breaking, the $SU(2)_{L,R}$ bosons $W^{\pm}_{L,R}$ mix and form the mass eigenstates $W^{\pm}_{1,2}$. In order to agree with weak interaction phenomenology, one has to require $W^{\pm}_1 = W^{\pm}(83\ \mathrm{GeV}) \simeq W^{\pm}_L$ and $W^{\pm}_2 \simeq W^{\pm}_R$ with $M_{W_R} \gg m_W$. Similar constraints hold for the neutral partners $Z^0_{1,2}$. The present lower bounds [7] on m_{W_R, Z_R} range from few hundred GeV to few TeV in the case of W_R. However, the more stringent bounds are also theoretically more uncertain. Thus, being cautious one cannot yet firmly rule out $M_{W_R, Z_R} \simeq$ O(300 GeV). This limit cannot be pushed very much farther at HERA. In the theoretically preferred case, that is for a heavy Majorana neutrino with $m_{\nu_R} \simeq M_{W_R}$, one is limited by phase space. On the other hand, one would have a spectacular signature: $\nu_R \to e^-X$ and e^+X with 50 % branching ratio for each channel. Unfortunately, the cross section is rather discouraging, $\sigma(ep \to \nu_R X) \simeq 0.1$ pb for $m_{\nu_R} \simeq M_{W_R} \simeq 180$ GeV. In the other extreme, for $m_{\nu_R} \lesssim$ O(few GeV) one can expect considerably larger rates as illustrated in Fig. 19. However, now the ν_R is most likely a Dirac fermion and one looses the nice signature. One way out is to show that $\sigma^{CC}(e^-_R p$ or $e^+_L p) \neq 0$ in contrast to the standard model expectation. This makes polarization mandatory. Unfortunately, with $P \simeq$ (60-80) % the background from ordinary left-handed weak interactions is big which decreases the sensitivity. [35] Nevertheless, the signal should be detectable if $M_{W_R} \lesssim$ 400 Gev. A similar conclusion can be drawn from Fig. 20 which shows the effect of the Z_R boson on a NC-asymmetry.

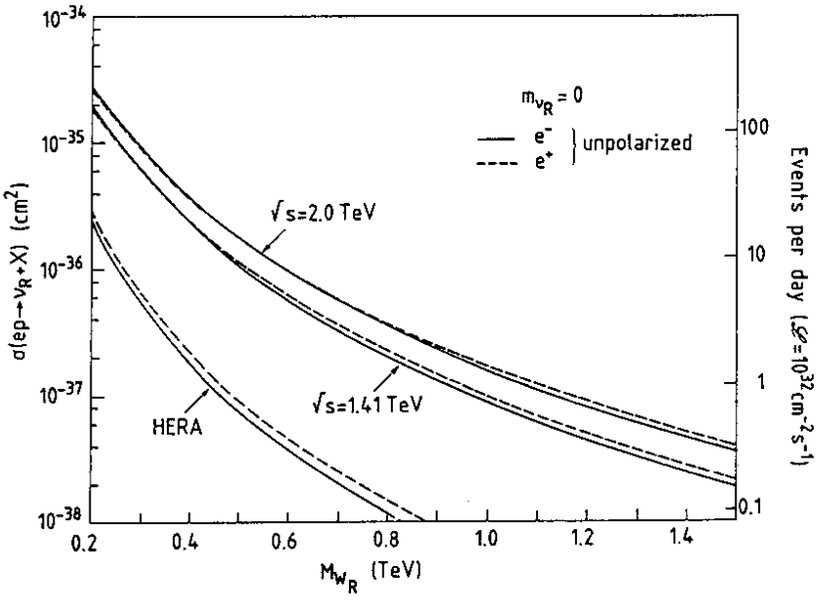

Fig. 19. Right-handed CC cross sections for the case of a very light right-handed neutrino (from ref. 3).

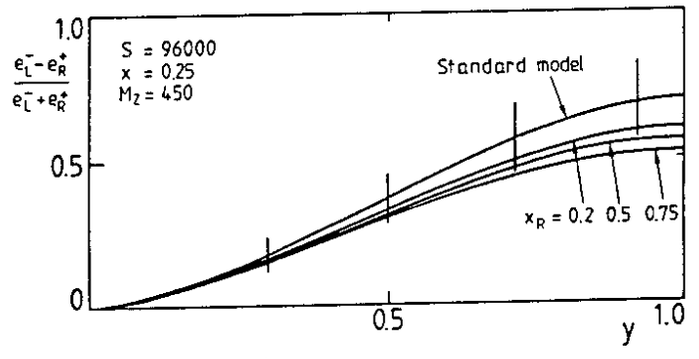

Fig. 20. Signal of a Z_R boson for M_{Z_R} = 450 GeV ($x_R = \sin^2\theta_R$, $y = Q^2/xs$). The experimental error corresponds to a run of 100 pb^{-1} for each polarization (from ref. 4).

5.4 Production of New Particles

As pointed out in 2., technicolor models [24] and composite models [25] of leptons and quarks typically predict massless Goldstone bosons associated with the spontaneous breaking of a global symmetry. Some of these become pseudo-Goldstone bosons by acquiring a radiative mass of $O(\alpha\Lambda)$ or $O(\alpha_s\Lambda)$ from standard $SU(3)_C \times SU(2)_L \times U(1)$ interactions. Particularly interesting species of this kind are the leptoquarks P, bosons which carry both lepton and quark internal quantum numbers. Technicolor models suggest [24] $m_P \simeq$ (100-200) GeV. The couplings to l's and q's are proportional to the fermion masses, $S_{lq} \frac{m_q - m_l}{\Lambda_{TC}} (\bar{q} l) P$ and involve unknown flavor mixing parameters S_{lq}. The latter make predictions on production rates rather

uncertain. Nevertheless, one may expect the processes drawn in Figs. 3b and 6a to constitute the most efficient sources of leptoquarks in ep collisions [47,48]. In both processes, the dominant contribution presumably comes from the coupling to the top flavor. Cross sections estimated from the diagram in Fig. 6a are shown in Fig. 21. The decay $P \to \tau \bar{t}$ followed by heavy flavor decays leads to final states with multilepton/jet and missing energy signatures. These signals can hardly be missed [4]. Thus, unless the production is very much suppressed by a small mixing parameter S_{et}, one should clearly be able to observe leptoquarks in the predicted mass range around 150 GeV if they exist. Note that production via γg-fusion (Fig. 8a) is not affected by flavor mixing, however, the cross section is moderate, to wit $\sigma(ep \to PPX) \simeq 0.1$ pb for $m_p \simeq 60$ GeV.

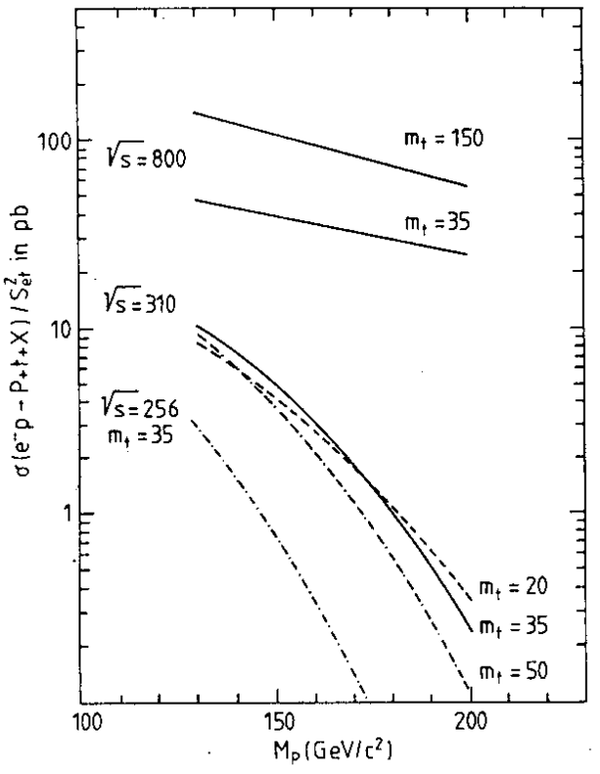

Fig. 21. Leptoquark production via diagram in Fig. 6a (from ref. 48).

Composite models of leptons and quarks also predict many excited fermions with conventional and exotic quantum numbers. Naively, one expects $m^* \sim O(\Lambda_H)$ which would preclude searches at HERA in case $\Lambda_H \gtrsim O(1\text{TeV})$ as suggested by Table 3. However, it is possible that the same mechanism which keeps the ground state fermions light, also leads to some relatively light excited states. If this is true, excited leptons and quarks can be produced at HERA with rather comfortable rates via the processes depicted in Figs. 5b and 6b. The most conventional case of a heavy electron with the same quantum numbers

as the ordinary electron is illustrated first. Gauge invariance requires a magnetic-type $e^* e \gamma$-coupling, while problems with (g-2) constraints can be avoided if this coupling is restricted to one helicity component of the electron: $\frac{e(f+f')}{2\Lambda} \cdot \bar{e}^* \sigma^{\mu\nu} e_L F_{\mu\nu}$. The results of a calculation[49] which also includes W and Z couplings are shown in Fig. 22. The cross section for e* production turns out to be rather favorable. Moreover, the decay $e^* \to e\gamma$ provides a very clean signature [4]. Similar rates as for the e* are obtained for excited quark production, $ep \to eq^*X$, if the results given in ref. 50 are rescaled in order to conciliate the different assumptions on the effective $f^* f \gamma$-coupling strength in refs. 49 and 50. Another interesting possibility is the production of color-octet electrons according to Fig. 6b. Again, one finds [51,2] big cross sections, for example, $\sigma(ep \to e_8 X) \simeq O(10\text{-}10^3)$ pb for $m_{e_8} \simeq 100$ GeV where the range reflects the theoretical uncertainty in the effective $e_8 eg$-coupling. In this case, the most obvious signature is a peak in the invariant e+jet mass distribution due to the decay $e_8 \to eg$. In conclusion, the prospects of excited fermion searches at HERA are very good.

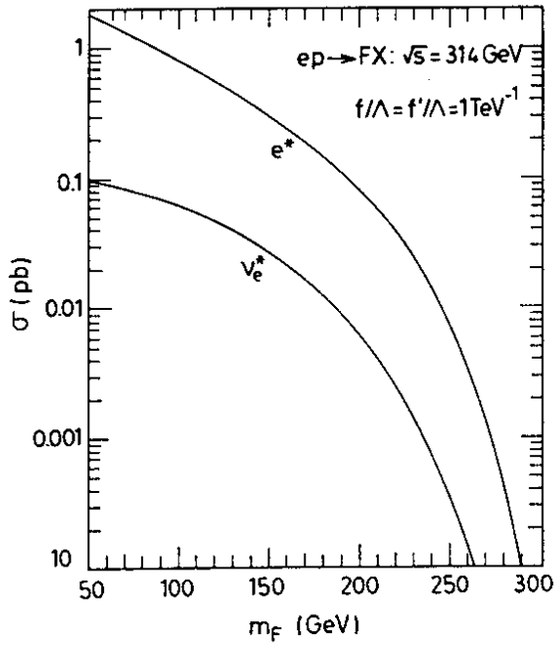

Fig. 22. Excited lepton production at HERA (from ref. 49)

The final example I want to consider is the production of SUSY particles (Table 1). Here, all couplings [52] are fixed by supersymmetry and gauge invariance. Unknown are only the masses of the SUSY particles and the mixing [52] of the weak eigenstates $(\tilde{W}^\pm, \tilde{H}^\pm)$ and

$(\tilde{B},\tilde{W}^3,\tilde{H}^0_{1,2})$ in the mass eigenstates $\tilde{\chi}^{\pm}_{1,2}$ and $(\tilde{\gamma}, \tilde{H}^0, \tilde{Z}^0_{1,2})$, respectively. The latter are called charginos and neutralinos, respectively. In the usual models [52], there is a discrete symmetry, called R-parity, which distinguishes ordinary particles (R = +1) from their superpartners (R = -1) and which is conserved multiplicatively. This has two important phenomenological consequences: firstly, SUSY particles can only be produced in pairs and, secondly, the lightest SUSY particle (in most models the $\tilde{\gamma}$ or $\tilde{H}^0$) is stable. Thus, SUSY events will always show missing energy and imbalance of transverse momentum. The most promising channels [53] to look for SUSY particles at HERA are $eq \to \tilde{e}\tilde{q}$ via neutralino exchange and $eq \to \tilde{\nu}\tilde{q}'$ via chargino exchange (see Fig. 3a). Fig. 23 summarizes the cross sections for $\tilde{e}\tilde{q}$ production as a function of $m_{\tilde{e}}$ and $m_{\tilde{q}}$. The uncertainty [54] due to neutralino mixing amounts to a factor 2 in both directions. One sees that $\sigma(eq \to \tilde{e}\tilde{q}) \simeq 0.1$ pb for $m_{\tilde{e}} + m_{\tilde{q}} \simeq 170$ GeV. It is relatively easy to detect this process if the photino is the lightest SUSY particle and $m_{\tilde{g}} > m_{\tilde{q}}$. In this case [4], the two-body decays $\tilde{e} \to e\tilde{\gamma}$ and $\tilde{q} \to q\tilde{\gamma}$ give rise to final states with a clear p_T-imbalance, and eq-correlations which are very different from the correlations in the standard NC process (Fig. 1). However, it is also quite possible [52] that the dominant decay modes are more complicated leading to multiparticle final states and, therefore, less striking missing energy signatures. For example, for $m_{\tilde{g}} < m_{\tilde{q}}$ one expects $\tilde{q} \to q\tilde{g}$, $\tilde{g} \to q\bar{q}\tilde{\gamma}$ to be the main decay chain. Thus, it should also be searched for multilepton/jet signatures. This is particularly advisable [4] in the case of $\tilde{\nu}\tilde{q}'$ pro-

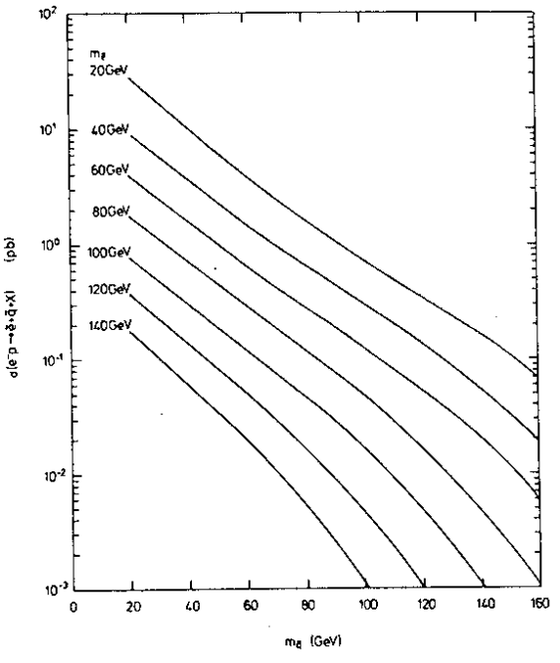

Fig. 23. Associated production of selectrons and squarks at HERA via $\tilde{\gamma}$ ($m_{\tilde{\gamma}}$ =0) and $\tilde{Z}^0$ ($m_{\tilde{Z}}$ = 95 GeV) exchange (from ref. 4).

duction since $\tilde{\nu} \to \nu\tilde{\gamma}$ may have a small branching ratio. Moreover, the decay products are invisible and, hence, it is more difficult to suppress the background from standard CC interactions (Fig. 1). The cross sections for $\tilde{\nu}\tilde{q}'$ production are of similar size as the ones shown in Fig. 23. However, the uncertainty [54] from chargino mixing is O(10). All other ways to produce SUSY particles at HERA are considerably less efficient. This applies to (i) squark production via $\gamma g \to \tilde{q}\bar{\tilde{q}}$ (Fig. 8a), (ii) squark-gluino production [55] via $\gamma q \to \tilde{q}\tilde{g}$ (Fig. 5a), and in particular to (iii) slepton-gaugino production [56], for example, via $e\gamma \to \tilde{e}\tilde{\gamma}$ (Fig. 5a). The largest accessible masses corresponding to a minimum cross section of 0.1 pb are as follows: (i) $m_{\tilde{q}} \simeq 60$ GeV, (ii) $m_{\tilde{q}} + m_{\tilde{g}} \simeq 80$ GeV and (iii) $m_{\tilde{e}} \simeq 30$ GeV if $(m_{\tilde{\gamma}} \simeq 0)$. Finally, indirect traces of supersymmetry [55,57] in the running of $\alpha_s(Q^2)$, the evolution of the structure functions, the longitudinal structure functions and other effects of this kind, are very difficult to detect, unless squarks or gluinos are very light, $\tilde{m} \lesssim$ O(few GeV). Note that the CERN $\bar{p}p$ collider data almost exclude such a possibility as can be seen from Table 2.

6. SUMMARY AND CONCLUSIONS

In this talk, I have discussed present prospects of physics at HERA from a theoretical point of view. The suggestions I presented are based on facts and on a belief. The facts are that the standard model successfully describes physics at present energies, but fails in a number of fundamental questions and that, because of these deficiencies, new physics must exist somewhere between the Fermi scale and the Planck mass. The belief (supported by good arguments) is that the energy scale of the new physics is so near that signals should be discovered at the next generation of accelerators.

I have briefly introduced the most popular ideas of how to supersede or complete the standard model: grand unification, supersymmetry and compositeness. Because of the total lack of experimental hints,

one does really not know which one, if anyone, of these suggestions has some truth in it. However, the existing models can serve as a guidance how to find out.

Quite generally, all these models predict small deviations from the standard theory at energies far below the new scale and rather clear signals if one comes sufficiently close. Since the new scale is unknown, future experiments have two complementary tasks: tests of the standard model to the highest possible accuracy and dedicated searches for "exotic" events.

HERA offers many ways to put the standard model to test in a new energy domain, most notably, by

- probing the proton structure at high Q^2,
- checking the correct running of α_s and the pattern of scaling violations over a large range in Q^2,
- investigating hard QCD scattering processes,
- studying electroweak properties, simultaneously in NC & CC processes and with polarized $e^{\pm}$-beams.

One can be confident of very stringent results if data from HERA, the new e^+e^- colliders, Tevatron and existing data are combined.

HERA can also probe the existence of new physics directly by searching for

quark form factors	:	$\Lambda \lesssim$ 300 GeV
residual interactions	:	$\Lambda \lesssim$ 3-5 TeV
new weak bosons	:	$m \lesssim$ 400 GeV
leptoquarks	:	$m \lesssim$ 200 GeV
excited fermions	:	$m \lesssim$ 200 GeV
SUSY particles	:	$m_{\tilde{e}} + m_{\tilde{q}} \lesssim$ 200 GeV

The numbers given above indicate the maximum accessible scales and masses guessed from the model studies I have presented. Most of the estimates involve considerable theoretical uncertainties: I have tried

to be realistic but not pessimistic. Comparison with the present bounds summarized in Table 2 and 3 shows that HERA can push some limits farther up, or find a signal. Of course, new bounds (or discoveries) can be expected from Tevatron, SLC and LEP I before HERA starts running. However, the physics at these colliders is complementary in some respects [58]. Concerning new particle search, ep collisions are optimal for discovering particles which carry the electron lepton number.

As a final remark, HERA is the only ep collider, at least in the foreseeable future, and therefore also technologically a unique adventure.

REFERENCES

1) Wiik, B. "Progress with HERA", DESY report HERA 85/16 (1985).

2) For an extended version of the present review see
Rückl, R. "The Physics Case of HERA", to appear in Proc. XIII. Int. Winter Meeting on Fundamental Physics, Cuenca, Spain, 1985.

3) Altarelli, G., Mele, B. and Rückl R., Proc. ECFA-CERN Workshop on Large Hadron Collider in the LEP Tunnel, ed. Jacob, M., CERN report 84-10, 551 (1984).

4) Cashmore, R.J. et al. "Exotic Phenomena in High Energy ep Collisions", Phys. Rep. 122, 275 (1985).

5) More detailed and extensive discussions, in particular, of experimental aspects can be found in the DESY reports HERA 81/18 (1981), 83/20 (1983) and 85/01 (1985).

6) Langacker, P., Proc. XXII. Int. Conf. on High Energy Physics, ed. Meyer, A. and Wieczorek, E. (Akad. der Wiss. der DDR, Zeuthen, 1984) Vol.II, p. 215.

7) For a recent review and further reference see
Langacker, P. "Unified Theories: Electroweak and GUT", UPR-0288T (1985), to appear in Proc. 1985 Int. Symp. on Lepton and Photon Interactions at High Energies, Kyoto, Japan.

8) Glashow, S.L., Nucl. Phys. 22, 579 (1961);
Weinberg, S., Phys. Rev. Lett. 19, 1264 (1967);
Salam, A., in Elementary Particle Theory: Relativistic Groups and Analyticity (Nobel Symposium No. 8), ed. Svartholm, N. (Almqvist and Wiksell, Stockholm, 1968) p. 367.

9) Coleman, S. and Weinberg, E., Phys. Rev. D7, 1888 (1973).

10) Guth, A. and Weinberg, E., Phys. Rev. Lett. 45, 1131 (1980); Witten, E., Nucl. Phys. B117, 477 (1981).

11) Veltman, M., Acta Phys. Pol. B8, 475 (1977).

12) Lee, B.W., Quigg, C. and Thacker, H., Phys. Rev. D16, 1519 (1977).

13) For a recent discussion see Gaillard, M.K. "Aspects of the Physics of Strongly Interacting W's and Z's, CERN-TH.4229/85 (1985), to appear in Proc. 1985 Theoretical Advanced Study Institute, Yale University.

14) Llewellyn Smith, C.H., Phys. Lett. 46B, 233 (1973); Bell, J.S., Nucl. Phys. B60, 427 (1973); Cornwall, J.M., Levin, D.N. and Tiktopoulos, G., Phys. Rev. Lett. 30, 1268 (1973) and Phys. Rev. D10, 1145 (1974).

15) Dashen, R. and Neuberger, H., Phys. Rev. Lett. 50, 1897 (1983); Bég, M.A., Panagiotakopoulos, C. and Sirlin, A., Phys. Rev. Lett. 52, 883 (1984); Lindner, M. "Implications of Triviality for the Standard Model", MPI-PAE/PTh 52/85 (1985) and references therein.

16) 't Hooft, G., Proc. NATO Advanced Study Institute on Recent Developments in Gauge Theories, ed. 't Hooft, G. et al. (Plenum Press, New York, 1980) p. 135.

17) For a recent review and further references see Ellis, J. "Supersymmetry and Supergravity", CERN-TH. 4277/85 (1985), to appear in Proc. 1985 Int. Symp. on Lepton and Photon Interactions at High Energies, Kyoto, Japan.

18) For a recent review and further references see Peskin, M.E. "Physics in and above TeV Region: Technicolor and Composite", invited talk at the 1985 Int. Symp. on Lepton and Photon Interactions at High Energies, Kyoto, Japan, to appear in the Proceedings.

19) Reya, E. "Beyond the Standard Model", in these Proceedings.

20) Green, M.B. "Superstring", invited talk at the 1985 Int. Symp. on Lepton and Photon Interactions at High Energies, Kyoto, Japan, to appear in the Proceedings.

21) Witten, E., Nucl. Phys. B258, 75 (1985).

22) Barger, V., Deshpande, N.G. and Whisnant, K., Phys. Rev. Lett. 56, 30 (1986).

23) Komamiya, S. "Search for New Particles in e^+e^- Annihilation", HD-PY 86/01 (1986), to appear in Proc. 1985 Int. Symp. on Lepton and Photon Interactions at High Energies, Kyoto, Japan; Küster, H., Proc. 1985 Int. Europhysics Conf. on High Energy Physics, ed. Nitti, L. and Preparata, G. (European Physical Society, Petit Lancy, Switzerland, 1986) p. 71.

24) Farhi, E. and Susskind L, Phys. Rep. 74, 277 (1981).

25) Buchmüller, W., Acta Phys. Austriaca Suppl. XXVII, 517 (1985); Harari, H., Proc. DESY Theory-Workshop on Physics at the Fermi Scale, DESY report T-85-02, 120 (1985).

26) Kögerler, R. and Schildknecht, D. "On Electroweak Interactions within Subconstituent Models", CERN-TH.3231 (1982); Fritzsch, H., Kögerler, R. and Schildknecht D., Phys. Lett. 114B, 157 (1982).

27) Case, K.M. and Gasiorowicz, S., Phys. Rev. 125, 1055 (1962); Weinberg, S. and Witten, E., Phys. Lett. 96B, 59 (1980).

28) Buchmüller, W. and Wyler, D. "Effective Lagrangian Analysis of New Interactions and Flavor Conservation", CERN-TH. 4254/85 (1985).

29) Yamada, S., Proc. 1983 Int. Symp. on Lepton and Photon Interactions at High Energies, ed. Cassel, D.G. and Kreinick, D.L. (Newman Lab., Cornell University, Ithaca, N.Y., 1983) p. 525 and Proc. DESY Theory-Workshop on Physics at the Fermi-Scale, DESY report T-85-02, 147 (1985); see also ref. 23.

30) Jenni, P., Proc. DESY Theory-Workshop on Physics at the Fermi-Scale, DESY report T-85-02, 226 (1985).

31) Kuroda, M., Schildknecht, D. and Schwarzer, K.-H., Nucl. Phys. B261, 432 (1985); Buchmüller, W., Phys. Lett. 145B, 151 (1984); Baur, U. and Streng, K.H. "Phenomenology of Composite Colored Weak Bosons", MPI-PAE/PTh 50/84, revised (1984).

32) Aurenche, P. et al., Phys. Lett. 135B, 164 (1984) and Z. Phys. C24, 309 (1984).

33) Altarelli, G., Martinelli, G., Mele, B. and Rückl, R., Nucl. Phys. B262, 204 (1985).

34) Bates, R. and Ng, J.N. "Non-standard Higgs Scalar and Pseudoscalar Boson Production in ep and e^+e^- Colliders", TRIUMF-PP-57 (1985).

35) see e.g. Longo, E., DESY report HERA 83/20, 285 (1983).

36) Engelen, J.J., DESY report HERA 83/20, 241 (1983) and references therein.

37) Hinchliffe, I. "Collision Rates and New Physics", LBL-18572 (1984).

38) Bjorken, J.D., Phys. Rev. 129,1547 (1969).

39) Altarelli, G., Phys. Rep. 81, 1 (1982).

40) Altarelli, G. and Parisi, G., Nucl. Phys. B126, 298 (1977).

41) Voss, R. "Structure Functions: Deep Inelastic Scattering on Nucleons and Nuclei", in these Proceedings.

42) Rückl, R., in preparation.

43) Martin, J., DESY report HERA 85/01, 115 (1985).

44) Peccei, R.D. and Rückl, R., Phys. Lett. 84B, 95 (1979) and Nucl. Phys. B162, 125 (1980);
Manesis, E.K. and Papadopoulos, N.A., J. Phys. G 8, 7 (1982);
Rückl, R. and Streng, K.H., in preparation.

45) Eichten, E.J., Kane, K.D. and Peskin, M.E., Phys. Rev. Lett. 50, 811 (1983).

46) Rückl, R., Phys. Lett. 129B, 363 (1983) and Nucl. Phys. B234, 91 (1984).

47) Bagger, J.A. and Peskin, E.M., Phys. Rev. D31, 2211 (1985) and erratum.

48) Rudaz, S. and Vermaseren, J.A.M., CERN report TH-2961 (1981) and erratum.

49) Hagiwara, K., Zeppenfeld, D. and Komamiya, S., Z. Phys. C29, 115 (1985).

50) Kühn, J.H., Tholl, H.D. and Zerwas, P.M., Phys. Lett. 158B, 270 (1985).

51) Baur, U., Ph.D. Thesis, University of Munich (1985);
Abolins, M. et al., Proc. 1982 DPF Summer Study on Elementary Particle Physics and Future Facilities, ed. Donaldson, R., Gustafson R. and Paige, F. (AIP , 1982) p. 274 and reference 47.

52) Haber, H.E. and Kane, G.L., Phys. Rep. 117, 75 (1985).

53) Jones, S.K. and Llewellyn Smith, C.H., Nucl. Phys. B217, 145 (1983).

54) Harrison, P.R., Nucl. Phys. B249, 704 (1985).

55) Hinchliffe, I. and Littenberg L., Proc. 1982 DPF Summer Study on Elementary Particle Physics and Future Facilities, ed. Donaldson, R., Gustafson R. and Paige, F. (AIP, 1982) and reference 53.

56) Altarelli, G., Martinelli, G., Mele, B. and Rückl, R., Nucl. Phys. B262, 204 (1985);
Salati, P. and Wallet, J.C., Phys. Lett. 122B, 397 (1983). The cross section for $e\tilde{\gamma} \to \tilde{\gamma}\tilde{e}$ and $m_{\tilde{\gamma}} = 0$ is grossly overestimated in this paper.

57) Campbell, B.A., Ellis, J. and Rudaz, S., Nucl. Phys. B198, 1 (1982);
Antoniadis, I., Kounnas, C. and Lacaze, R., Nucl. Phys. B211, 216 (1983);
Kounnas, C. and Ross, D.A., Nucl. Phys. B214, 317 (1983) and reference 53.

58) Peccei, R.D. "Physics Possibilities of Lepton and Hadron Colliders", DESY 85-040 (1985), to appear in Proc. 5th Topic Workshop on $p\bar{p}$ Collider Physics, Saint Vincent, Italy, 1985.